Progress In Electromagnetics Research C, Vol. 68, 201–209, 2016

Efficient Higher-Order Analysis of Electromagnetic Scattering of Objects in Half-Space by Domain Decomposition Method with a Hybrid Solver

Lan-Wei Guo, Jun Hu*, Wan Luo, Lian-Ning Song, and Zaiping Nie

Abstract—Integral equation domain decomposition method (IE-DDM) with an efficient higher-order method for the analysis of electromagnetic scattering from arbitrary three-dimensional conducting objects in a half-space is conducted in this paper. The original objects are decomposed into several closed subdomains. Due to the flexibility of DDM, it allows different basis functions and fast solvers to be used in different subdomains based on the property of each subdomain. Here, the higher-order vector basis functions defined on curvilinear triangular patches are used in each subdomain with the flexibility of order selection, which significantly reduces the number of unknowns. Then a novel hybrid solver is introduced where the adaptive cross approximation (ACA) and the half-space multilevel fast multipole algorithm (HS-MLFMA) are integrated seamlessly in the framework of IE-DDM. The hybrid solver enhances the capability of IE-DDM and realizes efficient solution for objects above, below, or even straddling the interface of a half-space. Numerical results are presented to validate the efficiency and accuracy of this method.

1. INTRODUCTION

The method of moments (MoM) based on surface integral equation method with the kernel of a half-space dyadic Green's function is a popular approach to model the electromagnetic (EM) scattering from arbitrarily shaped objects in a half space [1–4]. In this method, the unknown surface currents are of great importance in the computation. For electrically large structures, traditional low-order bases defined on rectangular or triangular mesh [5] usually lead to a huge number of degrees of freedom (DOFs), which makes it challenging to store and solve the matrix equation. There are usually two ways to circumvent this difficulty. One is to use the higher-order bases to significantly reduce the number of unknowns, and the other is to use fast methods to reduce the memory requirements and computational complexity.

Compared to the low-order bases, the higher-order bases can be defined over relatively larger elements, and the DOFs as well as the number of field-source interactions can be significantly reduced. There are mainly two kinds of higher-order basis functions, the interpolatory bases [6] and the hierarchical bases [7]. Due to the flexibility of order selection and p-adaption scheme, hierarchical vector bases are usually preferred [8–10]. More recently, hierarchical divergence-conforming vector basis functions defined on curved triangular patches have received much attention due to their modeling capability and good orthogonality [11, 12]. In [13], higher-order hierarchical vector bases (HOHVB) defined on a uniform mesh are adopted in layered-media problems, where the orders are selected according to the location of the bases in the layered-media. However, when modeling multiscale

Received 4 August 2016, Accepted 2 October 2016, Scheduled 24 October 2016
* Corresponding author: Jun Hu (hujun@uestc.edu.cn).
The authors are with the School of Electronic Engineering, University of Electronic Science and Technology of China (UESTC), Chengdu 611731, China.

structures, the mesh sizes in different parts are in high contrast. Therefore, a more pervasive and easier way of local order selection is needed.

On the other hand, a fast solver for general half-space scattering problem should be investigated carefully. The half-space multilevel fast multipole algorithm (HS-MLFMA) based on real-image approximation was introduced to the case when the object is located above or below a half-space [14]. In this manner, both the direct interaction Green's function and reflection-type (R-type) Green's function can be accelerated by using MLFMA, leading to an $O(N \log N)$ computational complexity. Unfortunately however, the transmission-type (T-type) Green's function cannot be handled in this way. Therefore, this method is restricted to the case when the objects are located completely in one layer. Due to their Green's function dependency, fast algorithms based on fast Fourier transform (FFT) [15] have similar restriction to MLFMA in half space problems. To remove this restriction, the kernel-independent adaptive cross approximation (ACA) algorithm [16, 17] was extended for general half-space problems. However, the computational complexity of ACA for dynamic problems is $O(N^{4/3} \log N)$, which is higher than MLFMA and FFT-based fast solvers. Recently, by sorting the basis function list, a hybrid fast solver was proposed in [18] for PEC bodies straddling a half-space interface. However, the sorting list is based on a z-dependent grouping scheme, which is not a universally applicable method.

Recently, a tear-and-interconnect domain decomposition method (DDM) was extensively studied because of its considerable flexibility in the meshing and effective preconditioning for complex problems exploiting iterative solutions [19–23]. In this approach, the surface of a non-penetrable perfect electrically conducting (PEC) object is decomposed into a set of closed subdomains, and transmission conditions (TCs) on touching faces are employed to enforce the continuity of currents across the interfaces. Thanks to the domain decomposition, it allows different bases and fast solvers to be used in different subdomains [10, 24]. In this work, an extension of the IE-DDM is developed for the modeling of electromagnetic scattering from arbitrary three-dimensional conducting objects above, below, or even straddling the interface of a half-space. Since each subdomain can be meshed independently, the HOHVB with the flexibility of order selection can be used in each subdomain independently. To further accelerate the computation, a novel hybrid solver sharing the efficiency of half-space MLMFA and the flexibility of ACA is integrated seamlessly in the framework of IE-DDM. Several examples in the applications of half-space problems are demonstrated to validate the efficiency and accuracy of this method.

2. FORMULATIONS AND EQUATIONS

2.1. IE-DDM with Higher-Order Basis Function in Half-Space Problems

For the sake of simplicity, a PEC cylinder above a half space is considered here. The permittivity and permeability of the lower layer are denoted as ϵ_1 and μ_1, respectively. The upper layer is always set as air, namely $\epsilon_0 = \mu_0 = 1$. The interface separating the two layers is set to $z = 0$. The whole computation domain Ω is first divided into two non-overlapping subdomains Ω_1 and Ω_2 as illustrated in Fig. 1, where $\Omega = \Omega_1 + \Omega_2$. We denote the artificial interface between two adjacent surfaces $\partial\Omega_1$ and $\partial\Omega_2$ as $\Gamma_{21} := \partial\Omega_1 \bigcap \partial\Omega_2$, where $\partial\Omega$ is the exterior boundary of each subdomain. According to Stratton-Chu representation formula, the tangential electric and magnetic fields on the boundary of

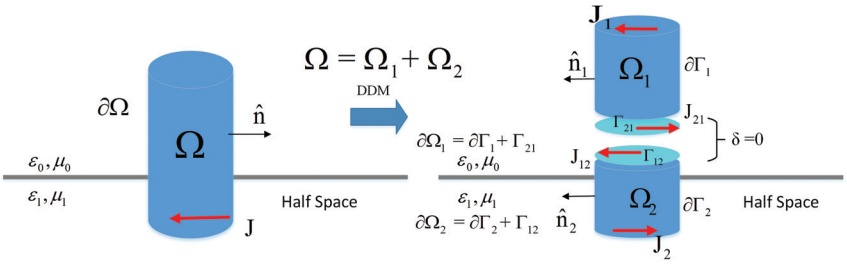

Figure 1. A decomposition of the PEC cylinder with touching surfaces.

each equivalent problem k can be expressed as:

$$\mathbf{E}_l(\mathbf{J}_l;\partial\Omega_l)(\mathbf{r}) := \eta_l\left[\hat{\mathbf{n}}_l \times \mathcal{L}_E(\mathbf{J}_l;\partial\Omega_l)(\mathbf{r}) \times \hat{\mathbf{n}}_l\right] \tag{1}$$

$$\mathbf{H}_l(\mathbf{J}_l;\partial\Omega_l)(\mathbf{r}) := \eta_l\left[-\hat{\mathbf{n}}_l \times 0.5\mathbf{J}_l + \hat{\mathbf{n}}_l \times \bar{\mathcal{K}}_H(\mathbf{J}_l;\partial\Omega_l)(\mathbf{r}) \times \hat{\mathbf{n}}_l\right] \tag{2}$$

where $\mathbf{J}$ is the induced surface current, and $\hat{\mathbf{n}}_k$ denotes the outward unit normal at the exterior surfaces. $\eta_l = \sqrt{\mu_l/\epsilon_l}$ and $k_l = \omega\sqrt{\mu_l\epsilon_l}$ are the intrinsic impedance and wavenumber in each subdomain. $\mathcal{L}$ and $\mathcal{K}$ denote respectively the well-known electric field integral operator (EFIO) and magnetic field integral operator (MFIO), and $\bar{\mathcal{K}}$ is the Cauchy principal value integration of $\mathcal{K}$.

$$\mathcal{L}_E(\mathbf{r},\mathbf{r}') = -j\omega\int d\mathbf{r}'\overline{\boldsymbol{G}}_e(\mathbf{r},\mathbf{r}')\mu(\mathbf{r}'). \tag{3}$$

$$\mathcal{K}_H(\mathbf{r},\mathbf{r}') = \underline{P.V.}\int d\mathbf{r}'\nabla\times\overline{\boldsymbol{G}}_e(\mathbf{r},\mathbf{r}'). \tag{4}$$

The integration kernel is the electric-type dyadic Green's function in a half space, which can be expressed as [2]:

$$\overline{\boldsymbol{G}}_e(\mathbf{r},\mathbf{r}') = \overline{\boldsymbol{G}}^D(\mathbf{r},\mathbf{r}') + \overline{\boldsymbol{G}}_e^R(\mathbf{r},\mathbf{r}') \tag{5}$$

where $\overline{\boldsymbol{G}}^D$ represents the direct term with an analytic solution in the absence of the half-space interface, and $\overline{\boldsymbol{G}}_e^R$ is the reflection term. It should be noted that the latter is polarization dependent and is usually expressed as a series of Sommerfeld integrals [25].

The combined field integral equation (CFIE) by weighted summation of EFIE and MFIE is adopted here to overcome the spurious internal resonance. To apply the higher-order technique, each subdomain is discretized into curvilinear triangular patches independently, and high mesh quality can be easily realized in each subdomain. With a local parametric coordinate system (ξ_1,ξ_2,ξ_3), where $0 \le \xi_1,\xi_2,\xi_3 \le 1$ and $\xi_1+\xi_2+\xi_3 = 1$, an arbitrary point on the curvilinear triangular patch can be easily determined by a mapping from the normalized parametric triangular patch with a polynomial equation. The unknown surface currents $\mathbf{J}_l$ on the subdomain l can be discretized by the HOHVB proposed in [12] as:

$$\mathbf{B}_e^{p,k} = E^{p,k}(\xi_1,\xi_2,\xi_3)\cdot\Lambda(\xi_1,\xi_2,\xi_3) \tag{6}$$

$$\mathbf{B}_f^{p,k} = F^{p,k}(\xi_1,\xi_2,\xi_3)\cdot\Lambda(\xi_1,\xi_2,\xi_3) \tag{7}$$

where $E^{p,k}$ and $F^{p,k}$ are edge-based and face-based p-th order hierarchical polynomials associated with the k-th edge. $\Lambda(\xi_1,\xi_2,\xi_3)$ is the well-known curvilinear RWG (CRWG) basis function [26]. The edge-based and face-based hierarchical polynomials up to the third order are summarized in Table 1, where $\psi_k = \xi_k - \xi_{k+1}$. More detailed analysis and discussion of HOHVB can be found in [12, 13].

Table 1. Edge-based and face-based hierarchical polynomials up to the third order associated with the kth edge.

Edge-based polynominals	Face-based polynominal
$E^{0,k} = 1$	$F_0^{0,k} = 0$
$E^{1,k} = \sqrt{3}(\psi_{k+1})$	$F_1^{1,k} = 2\sqrt{3}\xi_k$
$E^{2,k} = \frac{\sqrt{5}}{2}(3\psi_{k+1}^2 - 1)$	$F_2^{2,k} = 2\sqrt{3}\xi_k(5\xi_k - 3)$, $F_3^{2,k} = 6\sqrt{5}\psi_{k+1}\xi_k$
$E^{3,k} = \frac{\sqrt{7}}{2}(3\psi_{k+1}^3 - 3\psi_{k+1})$	$F_4^{3,k} = 2\sqrt{30}\xi_k(7\xi_k^2 - 8\xi_k + 2)$, $F_5^{3,k} = 2\sqrt{30}\psi_{k+1}\xi_k(7\xi_k - 3)$ $F_6^{3,k} = 2\sqrt{210}\xi_k(\psi_{k+1}^2 - 2\xi_{k+1}\xi_{k+2})$

To enforce the continuity of tangential field at the touching surfaces, the Robin transmission conditions (TCs) are employed:

$$\mathbf{J}_{12} = \mathbf{J}_{21} \tag{8}$$

By using the Robin TCs, independent meshing of different subdomains is allowed without requiring adjacent meshes to be continuous. That is to say, mesh density can be chosen according to the

geometrical characteristic of each subdomain. Consequently, HOHVB with flexibility of order selection can be applied in each subdomain conveniently.

By applying Galerkin test, an IE-DDM matrix equation can be obtained as

$$\mathbf{M}\mathbf{x} = \mathbf{b} + \mathbf{N}\mathbf{x} \tag{9}$$

and a robust block-diagonal (BD) preconditioning system can be derived as

$$\mathbf{M}^{-1}(\mathbf{M} - \mathbf{N})\mathbf{x} = \mathbf{M}^{-1}\mathbf{b} \tag{10}$$

In a two-domain case as shown in Fig. 1, (10) has the block structure as following:

$$\mathbf{M} - \mathbf{N} = \begin{pmatrix} \mathbf{M}_1 & 0 \\ 0 & \mathbf{M}_2 \end{pmatrix} - \left[\begin{pmatrix} \mathbf{B}_1 & \mathbf{D}_{21} \\ \mathbf{D}_{12} & \mathbf{B}_2 \end{pmatrix} + \begin{pmatrix} 0 & \mathbf{C}_1 \\ \mathbf{C}_2 & 0 \end{pmatrix} \right] \tag{11}$$

where $\mathbf{M}$ is a block diagonal matrix whose l-th block is the CFIE matrix for subdomain Ω_l, $\mathbf{B}_l$ the correction matrix for subdomain Ω_l for the final IE-DDM matrix, $\mathbf{C}_l$ the mutual coupling matrix between two subdomains, and $\mathbf{D}_l$ the cement matrices enforcing the transmission condition. Detailed expressions of these matrix blocks for free-space case can be found in [10, 19]. The counterpart in a half-space can be deduced similarly and will not be repeated here.

2.2. Hybrid Solver of MLFMA-ACA in IE-DDM

As introduced, the kernel-dependent fast solvers such as MLFMA have certain limitations in a half-space problem. A kernel-independent algebraic fast solver is usually more favorable when the object is straddling the interface of a half-space. Recently, the popular kernel-independent ACA was extended for such general half-space problems [17]. However, this method is less efficient than the kernel-dependent methods such as HS-MLFMA or FFT. To achieve an optimal efficiency, a novel hybrid solver in different subregions sharing the efficiency of half-space MLMFA and the flexibility of ACA is integrated seamlessly in the framework of IE-DDM.

Taking the two-domain case for example, the hybrid scheme for IE-DDM in Equations (9) and (10) is illustrated in Fig. 2. Here, HS-MLFMA and ACA are used in subdomain Ω_1 and subdomain Ω_2, respectively. In both algorithms, the interactions are classified into the near-region couplings that are computed directly and the well-separated couplings that are accelerated by the fast solvers. Because the accuracy of the real image for R-type Green's function deteriorates when the source point gets close to the interface, a buffer region is needed for HS-MLFMA when the object is close to or straddling the interface. Here the distance away from the interface for buffer region is denoted as ∇h_U and ∇h_L for the upper and lower layers, respectively.

Subdomain Ω_1 is in the upper layer and has a distance ∇h_U away from the interface. Thus the far interactions of the the self-interactions $\mathbf{M}_1^{\text{Far}}$ in each level are accounted for by an aggregation, translation, and disaggregation process [14]

$$\mathbf{M}_1^{\text{Far-MLFMA}}(m,n) = \oint d^2\hat{k}\mathbf{V}_{fm}(\hat{k}) \left[\alpha_{mn}(\hat{k})\mathbf{V}_{sn}(\hat{k}) + \alpha^I_{mn}(\hat{k})\overline{\boldsymbol{R}}(\hat{k})\mathbf{V}^i_{sn}(\hat{k}) \right] \tag{12}$$

(a) The hybrid solver for self-interactions (b) ACA for mutual couplings in different-side interactions

Figure 2. The hybrid solver for the two subdomains after domain decomposition of the original PEC structure in Fig. 1. Two octal-trees are used for different equivalent problems, which encloses the corresponding subdomain l ($l = 0, 1, 2$). The red solid line denotes octal-tree for HS-MLFMA, while the dotted line is for ACA. (a) Individual octal-tree which is used for the computation of $[\mathbf{M}_l][\mathbf{b}_k]$; (b) ACA octal-tree which is used for the computation of $[\mathbf{C}_l][\mathbf{b}_l]$.

where m and n denote the testing and basis functions in the observation and source groups; $\overline{\boldsymbol{R}}$ is the reflection dyad in the real-image approximation; superscript I stands for image. Detailed implementation of a standard HF-MLFMA can be found in [14] and will not be repeated here.

Subdomain Ω_2 is in the buffer region. Therefore, the far interactions of self-interactions of $\mathbf{M}_2^{\text{Far}}$ between two well-separated groups can be termed as

$$\mathbf{M}_2^{\text{Far-ACA}}(i \times j) \approx \mathbf{U}(i \times r) \cdot \mathbf{V}(r \times j) \tag{13}$$

where i and j denote the numbers of the testing and basis functions in the observation and source groups, respectively. r is the effective rank of the submatrix $\mathbf{M}_2^{\text{Far-ACA}}(i \times j)$. Detailed implementation of a standard ACA can be found in [16, 17].

For mutual coupling matrix $\mathbf{C}_l$, the hybrid solver should be investigated carefully. HS-MLFMA is used for source and field subdomains which are away from the interface and located completely in one layer. ACA is used when at least one subdomain is in the buffer region (close to the interface), or the two are in different layers.

Based on the philosophy of "divide and conquer", we combine the advantages of HOHVB, HS-MLFMA and ACA in the framework of domain decomposition for general half-space problems. For convenience, the method proposed in this paper is denoted as HOHVB-DDM, while the low-order analysis is denoted as CRWG-DDM. It will be shown in the numerical section that HOHVB-DDM can achieve more flexible mesh generation, higher computational efficiency, and less memory requirement than the conventional lower-order method.

3. NUMERICAL RESULTS

In this section, several typical half-space problems are presented to demonstrate the superior performance of the proposed HOHVB-DDM. In all these examples, the upper medium is set to be air, and λ_1 and λ_2 are the wavelengths in the upper and lower media, respectively.

In the first numerical example, a PEC cylinder with $D = 3\,\text{m}$ penetrating into the ground (with permittivity $\epsilon_r = 30$ and conductivity $\sigma = 0.05\,\text{S/m}$) is investigated to validate the proposed HOHVB-DDM. As depicted in the inset of Fig. 3(a), the cylinder is partitioned into two subdomains. The heights of the upper and lower parts are $H = 6.4\,\text{m}$ and $h = 1.6\,\text{m}$. A $\hat{\phi}$-polarized plane wave is incident from $\theta_{inc} = 60°$ and $\phi_{inc} = 90°$. The working frequency is 0.2 GHz, corresponding to $\lambda_1 = 1.5\,\text{m}$ and $\lambda_2 = 0.273\,\text{m}$. In the traditional lower-order method, the two parts should be meshed independently according to the wavelengths of their background layers, i.e., about $\lambda_1/10$ in the upper layer and $\lambda_2/10$ in the lower layer. Following this practice, the cylinder is discretized into 63,098 curvilinear

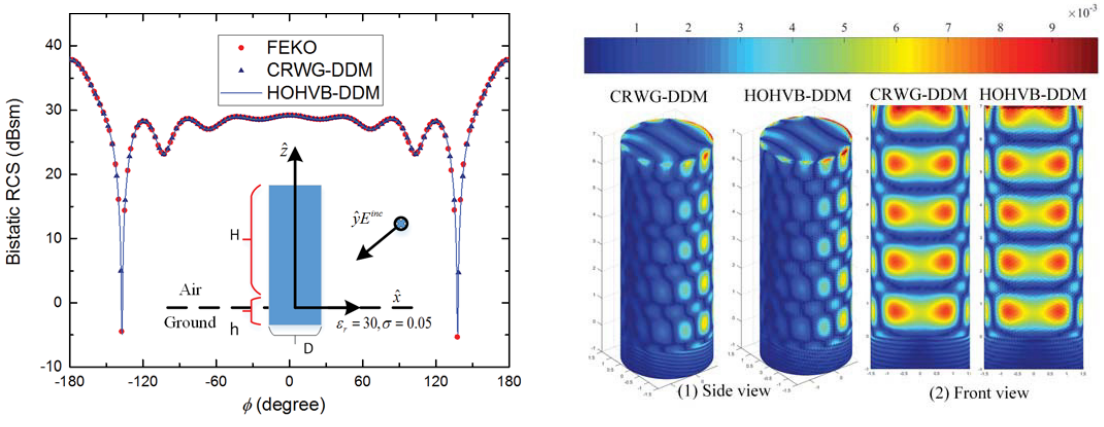

Figure 3. The cylinder example demonstrates the accuracy of HOHVB-DDM. (a) Bistatic RCS of the cylinder in the θ cut at 200 MHz with lower-order and higher-order methods, both of which are accelerated by the hybrid solver; (b) Real part of the equivalent current density.

triangular patches, which leads to 94,647 CRWG basis functions. However, in the higher-order method, the unknowns can be significantly reduced. Both subdomains are discretized by curvilinear triangular patch of $\lambda_1/4$. Choosing the basis order in the upper and lower subdomains to be 1 and 3 results in 8,940 DOFs, which is much smaller than the one in the traditional low-order method. To examine the accuracy of the proposed method, the bistatic radar cross section (RCS) along $\theta = 60^\circ$ cut and the induced electric currents are both calculated and shown in Fig. 3. Taking the results from FEKO simulation (based on RWG basis function) as a reference, good accuracy can be observed.

Table 2. Computational cost for solving the PEC cylinder penetrating into the ground.

Method	Unkonwns	Basis order for each subdomain	Memory (GB)	Totol time (hh)	Iter.num
MoM-RWG	77 901	0	45.2	26.7	61
CRWG-DDM-ACA	94 647	0	3.3	2.2	14
HOHVB-DDM-ACA	8 940	1;3	1.9	1.5	12
CRWG-DDM-HYS	94 647	0	2.5	1.6	14
HOHVB-DDM-HYS	8 940	1;3	1.2	1.1	12

The computational statistics are listed in Table 2 for comparison. Here CRWG-DDM-ACA and HOHVB-DDM-ACA denote that only ACA is used to accelerate the computation of IE-DDM matrix equations; CRWG-DDM-HYS and HOHVB-DDM-HYS denote that the hybrid solver of HS-MLFMA and ACA is used to solve the IE-DDM system. We find that the proposed HOHVB-DDM method can reduce the memory requirement and the solving time significantly. Moreover, the hybrid solver of HS-MLFMA and ACS also has a higher computational efficiency and lower memory requirement than the single ACA. Through this example, we have validated the accuracy and efficiency of the proposed method.

Table 3. Computational cost for solving the two NASA almonds.

Method	Unkonwns	Basis order for each subdomain	Memory (GB)	Totol time (h)	Iter.num
CRWG-DDM-ACA	223 323	0	19.1	14.2	17
HOHVB-DDM-ACA	35 963	0;2;0;1;3;1	6.6	5.8	15
CRWG-DDM-HYS	223 323	0	5.4	6.2	17
HOHVB-DDM-HYS	35 963	0;2;0;1;3;1	3.1	3.3	15

In the second example, two NASA almonds located in different layers are investigated where the relative permittivity of the bottom layer is $\varepsilon_r = 6 - j0.6$. The length of the almond is 12.5 m. A plane wave working at 0.3 GHz is incident form $\theta = 60^\circ$, $\phi = 0^\circ$ with polarization angle $\eta = 90^\circ$. As shown in Fig. 4(a), each almond is divided into three subdomains, resulting in 6 subdomains in total. Since the geometry of an almond contains sharp details, dense mesh is needed in subdomains 1 and 4. For comparison, CRWG basis functions are generated with mesh size of 0.1 λ_1 leading to the number of unknowns of 223,323. In the higher-order analysis, 0-th order basis with mesh size of 0.125 λ_1 is used in subdomains 1 and 3; 2nd order and 3rd order HOHVBs with mesh size of 0.45 λ_1 are used in subdomains 2 and 5; 1st order HOHVB with mesh size of $0.1\lambda_1$ is used in subdomains 4 and 6, respectively. The total number of unknowns of HOHVB is 35,963. In Fig. 4, the bistatic RCS and induced currents are computed by both lower-order and higher-order methods. As shown, good agreement can be observed. The computational cost is listed in Table 3, where high efficiency of the proposed hybrid method can be observed.

We study a more realistic problem in the last example. The geometrical model of the unexploded ordnance (UXO) is shown in Fig. 5. The length of the UXO is 5.84 m, and the diameter of the main

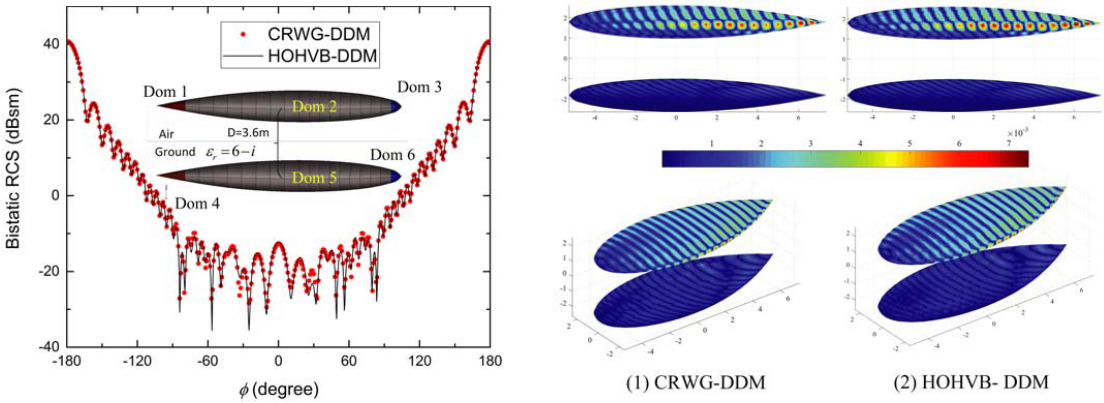

Figure 4. Two NASA almonds located in different layers. (a) Bistatic RCS of the NASA almonds in the θ cut at 300 MHz by using the lower-order and higher-order methods, both of which are accelerated by the hybrid solver of HS-MLFMA and ACA; (b) Real part of the equivalent current density.

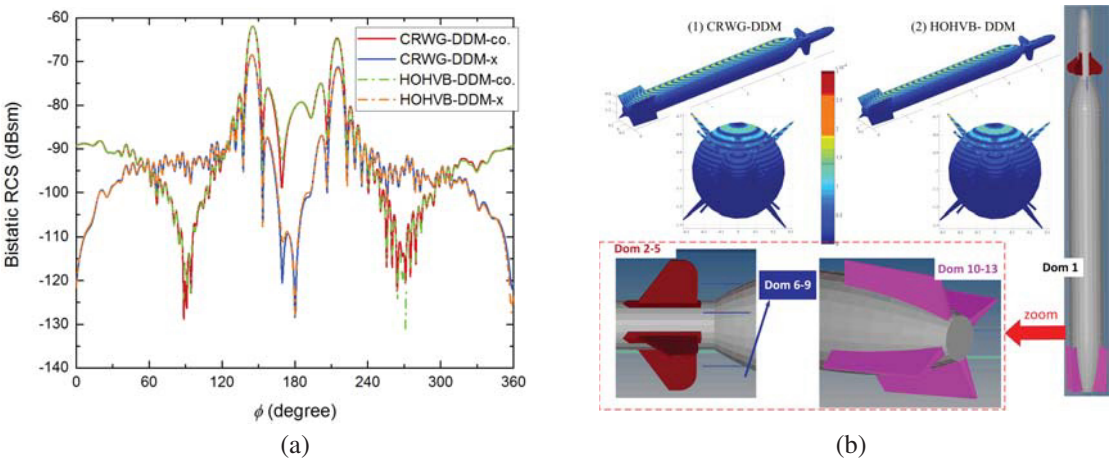

Figure 5. The scattering of UXO model. (a) Copolarized and cross-polarized RCSs of the UXO model calculated from the lower-order and higher-order methods, both of which are accelerated by HS-MLFMA; (b) Real part of the equivalent current density. The domain decomposition is also shown.

body is 0.53 m. It is buried in the soil with 20% water content, where the burying depth is 1.0 m. The working frequency is set to be 1.2 GHz, leading to an electrical length of $116.8\lambda_2$, where $\lambda_2 \approx 0.05$ m is the wavelength in the soil. The incident wave comes from $\theta = 45°$, $\phi = 0°$ with a polarization angle of $\eta = 0°$. As shown in Fig. 5(b), the UXO model is divided into 13 closed subdomains. For the lower-order bases with the minimum mesh size of $0.02\lambda_2$ and average mesh size of $0.1\lambda_2$, 1,215,762 CRWGs are generated. For the higher-order analysis, with the flexibility of order selection for each subdomain, only 262,815 unknowns are generated. The maximum and minimum sizes of HOHVB are $0.8\lambda_2$ and $0.02\lambda_2$,

Table 4. Computational cost for solving the UXO model buried 1.0 m under ground.

Method	Unkonwns	Basis order for each subdomain	Memory (GB)	Totol time (h)	Iter.num
CRWG-DDM	1 215 762	0	19.21	3.45	17
HOHVB-DDM	262 815	2,1,1,1,1,0,0,0,0,1,1,1,1	8.28	1.69	15

respectively. Since this object is electrically large and completely buried in the soil, only HS-MLFMA is adopted to accelerate the computation. Detailed computational statistics of CRWG-DDM and HOHVB-DDM are shown in Table 4. It can be observed that the higher-order technique significantly reduces the unknowns as well as the number of field-source interactions. Consequently, a higher efficiency can be achieved by using this higher-order method.

4. CONCLUSION

Hierarchical higher-order vector basis function is adopted and extended to IE-DDM to efficiently analyze the electromagnetic scattering from arbitrary three-dimensional conducting objects above, below, or even straddling the interface of a half-space. Here, higher-order bases defined on curvilinear triangular patches are used in each subdomains with the flexibility of order selection. This method significantly reduces the degrees of freedom as well as the number of field-source interactions in the simulation. Moreover, a novel hybrid solver sharing the efficiency of half-space MLMFA and the flexibility of ACA is employed in this paper. They are integrated seamlessly in the framework of IE-DDM. The proposed method not only facilitates the geometrical and electromagnetic modeling, but also provides a highly efficient and robust solver for general half-space problems.

ACKNOWLEDGMENT

This work is partially supported by Chang Jiang Scholar Project of MOE and the National Natural Science Foundation of China under Grant No. 61271033, No. 61231001, National Excellent Youth Fund by NSFC No. 61425010.

REFERENCES

1. Chew, W. C., *Waves and Fields in Inhomogeneous Media*, Van Nostrand Reinhold, 1990, Reprinted by IEEE Press, 1995.
2. Chen, Y. P., W. C. Chew, and L. Jiang, "A new Green's function formulation for modeling homogeneous objects in layered medium," *IEEE Trans. Antennas Propag.*, Vol. 60, No. 10, 4766–4776, Oct. 2012.
3. Michalski, K. A. and J. R. Mosig, "Multilayered media Green's functions in integral equation formulations," *IEEE Trans. Antennas Propag.*, Vol. 45, No. 3, 508–519, Mar. 1997.
4. Chen, Y. P., W. C. Chew, and L. Jiang, "A novel implementation of discrete complex image method for layered medium Green's function," *IEEE Antennas Wireless Propag. Lett.*, Vol. 10, 419–422, 2011.
5. Rao, S. M., D. R. Wilton, and A. W. Glisson, "Electromagnetic scattering by surfaces of arbitrary shape," *IEEE Trans. Antennas Propag.*, Vol. 30, No. 3, 409–418, 1982.
6. Graglia, R. D., D. R. Wilton, and A. F. Peterson, "Higher order interpolatory vector bases for computational electromagnetics." *IEEE Trans. Antennas Propag.*, Vol. 45, No. 3, 329–342, Mar. 1997.
7. Wang, J. and J. P. Webb, "Hierarchical vector boundary elements and p-adaption for 3-D electromagnetic scattering," *IEEE Trans. Antennas Propag.*, Vol. 47, No. 8, 1244–1253, Aug. 1997.
8. Jorgensen, E., O. S. Kim, P. Meincke, and O. Breinbjerg, "Higher order hierarchical discretization scheme for surface integral equations for layered media," *IEEE Trans. Geosci. Remote Sens.*, Vol. 42, No. 4, 764–772, Apr. 2004.
9. Lai, B., X. An, H. B. Yuan, N. Wang, and C. H. Liang, "AIM analysis of 3D PEC problems using higher order hierarchical basis functions," *IEEE Trans. Antennas Propag.*, Vol. 58, No. 4, 1417–1421, Apr. 2010.
10. Zhao, R., H. P. Zhao, Z. P. Nie, et al., "Fast integral equation solution of scattering of multiscale objects by domain decomposition method with mixed basis functions," *International Journal of Antennas and Propagation*, 1–7, 2015.

11. Graglia, R. D., A. F. Peterson, and F. P. Andriulli, "Curl-conforming hierarchical vector bases for triangles and tetrahedra," *IEEE Trans. Antennas Propag.*, Vol. 59, No. 3, 950–959, Mar. 2011.
12. Zha, L. P., Y. Q. Hu, and T. Su, "Efficient surface integral equation using hierarchical vector bases for complex EM scattering problems," *IEEE Trans. Antennas Propag.*, Vol. 60, No. 2, 952–957, Feb. 2012.
13. Luo, W., Z. Nie, and Y. P. Chen, "Efficient higher-order analysis of electromagnetic scattering by objects above, below, or straddling a half-space," *IEEE Antennas Wireless Propag. Lett.*, Vol. 15, 332–335, 2016.
14. Geng, N., A. Sullivan, and L. Carin, "Multilevel fast-multipole algorithm for scattering from conducting targets above or embedded in a lossy half space," *IEEE Trans. Geosci. Remote Sens.*, Vol. 38, No. 4, 1561–1573, Jul. 2000.
15. Millard, X. and Q. H. Liu, "Simulation of near-surface detection of objects in layeredmedia by the BCGS-FFT method," *IEEE Trans. Geosci. Remote Sens.*, Vol. 42, No. 2, 327–334, Feb. 2004.
16. Zhao, K., M. N. Vouvakis, and J. F. Lee, "The adaptive cross approximation algorithm for accelerated method of moments computations of EMC problems," *IEEE Trans. Electromagn. Compat.*, Vol. 47, No. 4, 763–773, Nov. 2005.
17. Luo, W., Z. Nie, and Y. Chen, "Fast analysis of electromagnetic scattering from three-dimensional objects straddling the interface of a half space," *IEEE Geosci. Remote Sens. Lett.*, Vol. 11, No. 7, 1205–1209, Jul. 2014.
18. Luo, W., Z. Nie, and Y. P. Chen, "A hybrid method for analyzing scattering from PEC bodies straddling a half-space interface," *IEEE Antennas Wireless Propag. Lett.*, Vol. 14, 474–477, 2015.
19. Peng, Z., X.-C. Wang, and J.-F. Lee, "Integral equation based domain decomposition method for solving electromagnetic wave scattering from non-penetrable objects," *IEEE Trans. Antennas Propag.*, Vol. 59, No. 9, 3328–3338, Sep. 2011.
20. Li, D., J. Wei, and J. F. Lee, "A new formulation discontinuous galerkin surface integral equation method for time-harmonic wave scattering problem," *IEEE International Symposium on Antennas and Propagation USNC/URSI National Radio Science Meeting*, 195–196, Vancouver, BC, CA, 2015.
21. Zheng, K. L., H. X. Zhou, and W. Hong, "Integral equation-based nonoverlapping DDM using the explicit boundary condition," *IEEE Trans. Antennas Propag.*, Vol. 63, No. 6, 2739–2745, Jun. 2015.
22. Echeverri Bautista, M. A., F. Vipiana, M. A. Francavilla, J. A. Tobon Vasquez, and G. Vecchi, "A nonconformal domain decomposition scheme for the analysis of multiscale structures," *IEEE Trans. Antennas Propag.*, Vol. 63, No. 8, 3548–3560, Aug. 2015.
23. Peng, Z., R. Hiptmair, Y. Shao, and B. Mackie-Mason, "Domain decomposition preconditioning for surface integral equations in solving challenging electromagnetic scattering problems," *IEEE Trans. Antennas Propag.*, Vol. 64, No. 1, 210–223, Jan. 2016.
24. Zhao, R., J. Hu, H. Guo, et al., "A hybrid solvers enhanced integral equation domain decomposition method for modeling of electromagnetic radiation," *International Journal of Antennas and Propagation*, 1–8, 2015.
25. Chen, Y. P., S. Sun, L. Jiang, and W. C. Chew, "A Calderon preconditioner for the electric field integral equation with layered medium Green's function," *IEEE Trans. Antennas Propag.*, Vol. 62, No. 4, 2022–2030, Apr. 2014.
26. Donepudi, K. C., K. Gang, J. M. Song, and W. C. Chew, "Higher-order MoM implementation to solve integral equations," *IEEE Antennas and Propagation Society International Symposium*, Vol. 3, 1716–1719, Orlando, FL, USA, 1999.